Biomedicine & Pharmacotherapy 150 (2022) 112940

Contents lists available at ScienceDirect

Biomedicine & Pharmacotherapy

journal homepage: www.elsevier.com/locate/biopha

A diphtheria toxin-based nanoparticle achieves specific cytotoxic effect on CXCR4$^+$ lymphoma cells without toxicity in immunocompromised and immunocompetent mice

Aïda Falgàs [a,b,c], Annabel Garcia-León [a,b], Yáiza Núñez [a,b], Naroa Serna [c,d,e], Laura Sánchez-Garcia [c,d,e], Ugutz Unzueta [a,b,c,d], Eric Voltà-Durán [c,d,e], Marc Aragó [a], Patricia Álamo [a,b,c], Lorena Alba-Castellón [a,b], Jorge Sierra [a,b,f,*], Alberto Gallardo [g], Antonio Villaverde [c,d,e], Esther Vázquez [c,d,e,**], Ramon Mangues [a,b,c,***], Isolda Casanova [a,b,c]

[a] Biomedical Research Institute Sant Pau (IIB-Sant Pau), Hospital de la Santa Creu i Sant Pau, Barcelona 08025, Spain
[b] Josep Carreras Leukaemia Research Institute (IJC), Barcelona 08916, Spain
[c] CIBER de Bioingeniería Biomateriales y Nanomedicina (CIBER-BBN), Madrid 28029, Spain
[d] Department of Genetics and Microbiology, Universitat Autònoma de Barcelona, Barcelona 08193, Spain
[e] Institute of Biotechnology and Biomedicine (IBB), Universitat Autònoma de Barcelona, Barcelona 08193, Spain
[f] Department of Hematology, Hospital de la Santa Creu i Sant Pau, Barcelona 08025, Spain
[g] Department of Pathology, Hospital de la Santa Creu i Sant Pau, Barcelona 08025, Spain

ARTICLE INFO

Keywords:
Targeted-drug delivery
Nanoparticle
Diphtheria toxin
CXCR4 receptor
DLBCL
Multivalency

ABSTRACT

High rates of relapsed and refractory diffuse large B-cell lymphoma (DLBCL) patients and life-threatening side effects associated with immunochemotherapy make an urgent need to develop new therapies for DLBCL patients. Immunotoxins seem very potent anticancer therapies but their use is limited because of their high toxicity. Accordingly, the self-assembling polypeptidic nanoparticle, T22-DITOX-H6, incorporating the diphtheria toxin and targeted to CXCR4 receptor, which is overexpressed in DLBCL cells, could offer a new strategy to selectively eliminate CXCR4$^+$ DLBCL cells without adverse effects. In these terms, our work demonstrated that T22-DITOX-H6 showed high specific cytotoxicity towards CXCR4$^+$ DLBCL cells at the low nanomolar range, which was dependent on caspase-3 cleavage, PARP activation and an increase of cells in early/late apoptosis. Repeated nanoparticle administration induced antineoplastic effect, *in vivo* and *ex vivo*, in a disseminated immunocompromised mouse model generated by intravenous injection of human luminescent CXCR4$^+$ DLBCL cells. Moreover, T22-DITOX-H6 inhibited tumor growth in a subcutaneous immunocompetent mouse model bearing mouse CXCR4$^+$ lymphoma cells in the absence of alterations in the hemogram, liver or kidney injury markers or on-target or off-target organ histology. Thus, T22-DITOX-H6 demonstrates a selective cytotoxicity towards CXCR4$^+$ DLBCL cells without the induction of toxicity in non-lymphoma infiltrated organs nor hematologic toxicity.

Abbreviations: ALT, alanine transaminase; AST, aspartate transaminase; AUC, area under the curve; BLI, bioluminescence imaging; BM, bone marrow; CLS, capillary leak syndrome; DLBCL, diffuse large B-cell lymphoma; FDA, Food and Drug Administration; H&E, hematoxylin and eosin; IHC, immunohistochemistry; IV, intravenous; LN, lymph node; MFI, mean fluorescence intensity; PARP, poly (ADP-ribose) polymerase; PLT, platelets; RBC, red blood cells; SC, subcutaneous; WBC, white blood cells.

* Correspondence to: Biomedical Research Institute Sant Pau (IIB-Sant Pau), Josep Carreras Leukaemia Research Institute (IJC) and Department of Hematology, Hospital de la Santa Creu i Sant Pau, Barcelona, Spain.

** Correspondence to: Department of Genetics and Microbiology (Universitat Autònoma de Barcelona) and Institute of Biotechnology and Biomedicine (IBB) , Barcelona, and CIBER de Bioingeniería Biomateriales y Nanomedicina (CIBER-BBN), Madrid, Spain.

*** Correspondence to: Biomedical Research Institute Sant Pau (IIB-Sant Pau) and Josep Carreras Leukaemia Research Institute (IJC), Barcelona, and CIBER de Bioingeniería Biomateriales y Nanomedicina (CIBER-BBN), Madrid, Spain.

E-mail addresses: jsierra@santpau.cat (J. Sierra), esther.vazquez@uab.cat (E. Vázquez), rmangues@santpau.cat (R. Mangues).

https://doi.org/10.1016/j.biopha.2022.112940
Received 21 February 2022; Received in revised form 27 March 2022; Accepted 6 April 2022
Available online 11 April 2022

1. Introduction

Diffuse large B cell lymphoma (DLBCL) is the most common subtype of non-Hodgkin lymphoma accounting around 30–40% of all cases [1]. First-line therapy for these patients combines the monoclonal antibody anti-CD20 (rituximab) with cyclophosphamide, doxorubicin, vincristine, and prednisone (R-CHOP). Nevertheless, between 40% and 50% of DLBCL patients relapse or have refractory disease [2,3]. R-CHOP is the common treatment for DLBCL and combines Rituximab immunotherapy with chemotherapy agents that damage the DNA or microtubule-destabilizing agents that kill dividing cells but spare non-dividing cells [4]. Moreover, chemotherapy passively diffuses through all organs killing both tumor cells and normal cells. For this reason, patients can experience severe side effects, including life-threatening effects such as bone marrow (BM) myelosupression, cardiotoxicity or neurotoxicity [5–8]. Thus, targeted therapeutic approaches are needed aiming to increase the cytotoxicity of lymphoma cells whereas reducing the off-target toxicity.

Bacterial toxins are increasingly used as potent anticancer agents due to their high cytotoxicity and they are usually linked to a monoclonal antibody (as immunotoxins) that confers them the specificity towards a target molecule in order to reduce the unspecific toxicity. Three immunotoxins have been approved by the Food and Drug Administration (FDA), denileukin diftitox, moxetumomab pasudotox and tagraxofusp-erzs, containing a monoclonal antibody conjugated to a toxin payload, either the diphtheria or the *Pseudomonas aeruginosa* toxin [9–12]. However, the possible drug leakage in the bloodstream and the small amount of the injected dose (<1%) reaching the tumor can limit the development of immunotoxins [13,14].

Taking into account the risks and limitations of immunotoxins, we developed a new strategy based on a self-assembling toxin-based nanoparticle named T22-DITOX-H6, with a size over 30 nm. The nanoparticle is composed of monomers, each being constructed by a single polypeptide chain that includes the translocation and catalytic domains of the diphtheria toxin. Moreover, this nanoparticle construct includes a hexa-histidine tail (H6) for nanoparticle purification by affinity chromatography and the T22 ligand for the targeting to CXCR4 receptor. Our group reported that CXCR4 is a good target for DLBCL patients since CXCR4 overexpression is found in around 30–50% of DLBCL patient samples [15,16]. Moreover, CXCR4 overexpression in DLBCL patients is involved in relapse and resistance to R-CHOP and confers them poor progression-free survival and overall survival [15–18]. Furthermore, the nanoparticle includes a natural furin-cleavage site between the T22 ligand and the toxin domains for the release of the toxin once internalized into target cells, as well as another furin-cleavage site that separates the catalytic domain from the translocation domain, allowing to exert its cytotoxic function into target cells. Once into the cytoplasm, the catalytic domain inactivates protein synthesis to induce cell death [19,20].

In this work, we aim at evaluating the specific *in vitro* cytotoxic effect of T22-DITOX-H6 in human and murine CXCR4$^+$ DLBCL cells as well as the *in vivo* anti-lymphoma effect and on-target as well as off-target toxicity using both xenograft immunocompromised and immunocompetent mice. Thus, we expect that the combination of our compact and multivalent T22-DITOX-H6 nanoparticle, with its active targeting to CXCR4-overexpressing lymphoma cells and the potent mechanism of action of diphtheria toxin, will make for an effective and safe strategy to eliminate CXCR4$^+$ DLBCL cells.

2. Material and methods

2.1. Therapeutic T22-DITOX-H6 nanoparticle construction

The T22-DITOX-H6 nanoarchitecture, production and purification were described in our previous work [20].

2.2. Cell culture

Human Toledo and U-2932 DLBCL cell lines were cultured with RPMI 1640 medium whereas the human SUDHL-2 DLBCL cell line was cultured in IMDM medium. All cell lines were supplemented with 10% fetal bovine serum (FBS), 1% glutamine and 100 U/mL penicillin-streptomycin (Thermo Fisher Scientific, Waltham, MA, USA). Toledo cell line was purchased from the American Type Culture Collection (ATCC, Manassas, Virginia, USA) and U-2932 cell line from the German Collection of Microorganisms and Cell Cultures (DSMZ, Braunschweig, Germany). Finally, SUDHL-2 cell line was kindly provided by Dr L. Pasqualucci (Columbia University, NY, USA) and its cell line identity was verified at genomics and transcriptomics platform at IIB-Sant Pau.

As reported in previous works [21,22], Toledo and U-2932 cells express high membrane CXCR4 levels whereas SUDHL-2 does not. The SUDHL-2 cell line was transfected by nucleofection (Nucleofector TM 2b Device, Lonza, Basel, Switzerland) with the pCXCR4 plasmid, kindly provided by Dr. Jun Komano (Osaka Prefectural Institute of Public Health, Osaka, Japan) and CXCR4 positive cells were selected with 0.4 mg/mL of geneticin (Thermo Fisher Scientific), resulting a new cell line named CXCR4$^+$ SUDHL-2. Furthermore, the Toledo cell line was nucleofected with the Luciferase gene (pPK-CMV- F3, Promokine, TE Huissen, The Netherlands) and the resulted Toledo-Luci cells were selected with 0.2 mg/mL of geneticin in order to achieve stable clones.

Additionally, the murine A-20 lymphoma cell line was cultured with RPMI 1640 medium, 10% FBS, 1% glutamine, 100 U/mL penicillin-streptomycin, 0.05 mM 2-mercaptoethanol (Sigma-Aldrich, Saint Louis, MO, USA) and 10 mM Hepes (Thermo Fisher Scientific). A-20 cell line was purchased from the ATCC.

2.3. Cell viability assays

Cell viability assays were used to assess the nanoparticle cytotoxicity in human and murine lymphoma cell lines. Lymphoma cells were seeded, in 96-well plates, from $2.5{\cdot}10^5$ to $3.5{\cdot}10^5$cells/mL depending on their growth rate. After 24 h, cells were exposed to different concentrations of T22-DITOX-H6 or buffer (166 mM $NaCO_3H$, pH=8). Moreover, for competition assays, aiming to test if nanoparticle entrance in cancer cells is mediated by the CXCR4 receptor, cells were pretreated with the CXCR4 antagonist AMD3100 (Sigma-Aldrich) 1 h before the nanoparticle addition (10 AMD3100: 1 T22-DITOX-H6 concentration ratio). Thus, cancer cell exposure to AMD3100 blocks its membrane CXCR4 receptors, leading to the inhibition of the internalization of the CXCR4-targeted nanotoxin. Evaluation of cell death caspase-dependence was performed adding z-VAD-FMK pancaspase inhibitor (Adooq Bioscience, Irvine, CA, USA) at 100 μM 1 h prior nanoparticle exposition.

Then, the colorimetric cell proliferation kit reagent (Roche Diagnostics, Basel, Switzerland) was added after 48 h of nanoparticle exposure and, after 4 h of incubation, cell viability was quantified by measuring the absorbance at 492 nm wavelength using a FLUOstar OPTIMA spectrophotometer (BMG Labtech, Ortenberg, Germany). Results were expressed as percentage of cell viability in relation to the corresponding vehicle control (negative controls, 100% of cell viability), *e.g.* cytotoxicity assays testing T22-DITOX-H6 alone, the vehicle control was the nanoparticle buffer (166 mM NaCO3H, pH=8); in competition assays the negative control was the AMD3100 together with the nanoparticle buffer and in cell death caspase-dependence assays, the negative control was zVAD-FMK together with the nanoparticle buffer.

2.4. Flow cytometry

For determining the membrane CXCR4 expression, cells were firstly washed with PBS 0.5% BSA. Then, human SUDHL-2 and CXCR4$^+$ SUDHL-2 cells were incubated with PE-Cy5 mouse anti-human CXCR4 monoclonal antibody (BD Biosciences, Franklin Lakes, NJ, USA) or PE-

Cy5 Mouse IgG2a isotype control antibody (BD Biosciences) and murine A-20 cells with PE anti-mouse CD184 (CXCR4) antibody (Biolegend, San Diego, CA, USA) or PE Rat IgG2b isotype control antibody (Biolegend). Incubation with antibodies was performed for 20 min at 4ºC followed by another PBS 0.5% BSA wash. Finally, cells were captured by FACS Calibur flow cytometry (BD Biosciences) and the results were analyzed using the Cell Quest Pro software and expressed as mean fluorescence intensity (MFI).

2.5. Western blot

Toledo and U-2932 cells were seeded in flasks at $3.5{\cdot}10^5$ and $3.0{\cdot}10^5$ cells/mL, respectively, and treated with buffer or 5 nM of T22-DITOX-H6 for 24 h and 48 h. For SUDHL-2 and $CXCR4^+$ SUDHL-2 extracts, cells were seeded at $2.5{\cdot}10^5$ and $3.0{\cdot}10^5$ cells/mL, respectively. Cells were washed twice with PBS and resuspended in lysis buffer (1 M Tris/acetate, 1 M sucrose, 100 mM EDTA, 100 mM EGTA, 10% TritonX-100, 100 mM Naorto, 100 mM Naβglycerol, 0.5 M NaF, 100 mM Napyro, 1% β-mercapto, 100 mM Benzamidine, 1.74 mg/mL PMSF and 2 mg/mL leupeptin). The cell suspension was sonicated and rested for 20 min on ice and, then, centrifuged for 10 min at 14,000 rpm and 4 ºC. Protein concentration in supernatant was determined using the Bradford protein assay, according to the manufacturer's instructions (BioRad). Cell lysates (50 μg) were mixed with LB6X-DTT 3 M, separated using 12–15% SDS-PAGE and transferred to a nitrocellulose blotting membrane (GE Healthcare life sciences). Membranes were blocked with 5% skim milk in TBST for 2 h at room temperature. Then, membranes containing Toledo and U-2932 cell lysates were incubated with the following primary antibodies: 1:2000 PARP (556494, BD Biosciences), 1:1000 caspase-3 (610322, BD Biosciences) and 1:1000 cleaved caspase-3 (9661, Cell Signaling Technology, Danvers, MA, USA); SUDHL-2 and $CXCR4^+$ SUDHL-2 membranes were incubated with 1:1000 CXCR4 (1009, Prosci, Fort Collins, CO, USA). The loading control antibody used was α/β tubulin (2148, Cell Signaling Technology) at 1:1000. Membranes were washed with TBST and then incubated with the appropriate secondary antibody (1:10,000, Jackson Immune Research). Western blot visualization was performed using the SuperSignal West Pico Chemiluminescent Substrate (Thermo Fisher Scientific) and the G:BOX iChemi XT Imaging System (Syngene).

2.6. Annexin/PI assay

Toledo and U-2932 cells were seeded at $3.5{\cdot}10^5$ and $3.0{\cdot}10^5$ cells/mL, respectively, and treated with buffer (166 mM $NaCO_3H$, pH=8) or 5 nM T22-DITOX-H6 for 15 h, 24 h or 48 h. The percentage of cell viability, early apoptosis and late apoptosis was evaluated using the Annexin V-CF Blue/PI apoptosis detection kit (Abcam, Cambridge, UK) and following the manufacturer's instructions. Data were analyzed by MACSQuant analyzer flow cytometry using the MACS Quantify version 2.3 software (Miltenyi Biotec, Bergisch Gladbach, North Rhine-Westphalia, Germany).

2.7. DAPI staining

Lymphoma cells were seeded from $2.5{\cdot}10^5$ to $3.5{\cdot}10^5$cells/mL depending on their growth rate and treated with buffer (166 mM $NaCO_3H$, pH=8) or 2.5 nM or 5 nM T22-DITOX-H6 for 48 h. After that time, cells were washed with PBS, incubated with 3.7% paraformaldehyde for 10 min at − 20 ºC, washed again and placed on a slide. Finally, these cells were stained with DAPI mounting medium (Thermo Fisher Scientific) and visualized using a fluorescence microscope (Olympus BX53, Olympus). Representative pictures were taken using an Olympus DP73 digital camera and processed with the cellSens Dimension 1.9 software (Olympus) at 1000X magnification.

2.8. Animal maintenance

Four-week-old female NOD/SCID mice and seven-week-old female BALB/cByJ mice were obtained from Charles River Laboratories (Wilmington, MA, USA). Mice were housed in microisolator units with sterile food and water ad libitum. All procedures were conducted in accordance with the guidelines approved by the institutional animal Ethics Committee of Hospital Sant Pau and performed following the European Union Directive 2010-63-EU for welfare of the laboratory animals.

2.9. In vivo T22-DITOX-H6 antineoplastic effect in Toledo-Luci disseminated mouse model

After one week of quarantine, eighteen immunocompromised NODSCID mice were intravenously injected with $20{\cdot}10^6$ Toledo-Luci cells. Three days later, mice were randomized and divided into two groups (n = 9/group), the control group was treated with buffer (166 mM $NaCO_3H$, pH=8) and the experimental group was treated with 10 μg T22-DITOX-H6. The treatment administration was performed intravenously three times per week in a total of thirteen doses. *In vivo* lymphoma dissemination was monitored using bioluminescence imaging (BLI) as total radiance photons in the IVIS Spectrum (Perkin-Elmer, Waltham, MA, USA). For that, mice were anesthetized with 3% isoflurane in oxygen and BLI was captured 5 min after intraperitoneal injection of firefly D-luciferin (2.25 mg/mouse, Perkin Elmer). In addition, mouse body weight was registered at least twice per week. All mice were euthanized the day that the first animal presented relevant signs of disease such as lack of mobility or 10% weight loss. At that day, the BLI signal from lymphoma-infiltrated organs was quantified *ex vivo* as average radiance photons and then all organs were embedded in paraffin for further histological analyses.

2.10. In vivo T22-DITOX-H6 antineoplastic effect in A-20 subcutaneous (SC) mouse model

After one week of quarantine, ten immunocompetent BALB/cByJ mice were subcutaneously injected with $5{\cdot}10^5$ A-20 cells. Tumor growth was monitored twice a week with bilateral caliper measurements ($width^2$ x length/2). When tumors reached a volume between 50 and 100 mm^3, mice were randomly divided in control group (n = 5), treated intravenously with 166 mM $NaCO_3H$, pH= 8 buffer, and experimental group (n = 4), treated intravenously with 5 μg T22-DITOX-H6. One mouse was excluded from the experiment because of technical problems during the intravenous injection. Mice were treated three times per week until the first mice achieved a tumor volume size of 500 mm^3. Then, animals were euthanized and all organs were embedded in paraffin for further histological analyses.

The area under the curve (AUC) of tumor size from buffer and nanoparticle-treated mice was calculated using the GraphPad Prism 6 program.

2.11. Paraffin-embedded cell blocks

A-20 cells were paraffin-embedded from the centrifuged cell suspension by adding five drops of plasma and thrombin to enmesh the cellular material in a clot. Then, cell clots were placed in a cassette, fixed in 4% paraformaldehyde and paraffin-embedded in a tissue processor (Sakura, Tokyo, Japan).

2.12. Hematoxilin and eosin (H&E) and immunohistochemical staining

Paraffin-embedded organs from immunocompromised and immunocompetent mice were analyzed histopathologically (H&E staining) by two independent observers to assess the possible toxicity.

CXCR4 (1:300, Abcam) expression was evaluated in cellular blocks. Immunohistochemistry staining was performed in a DAKO Autostainer

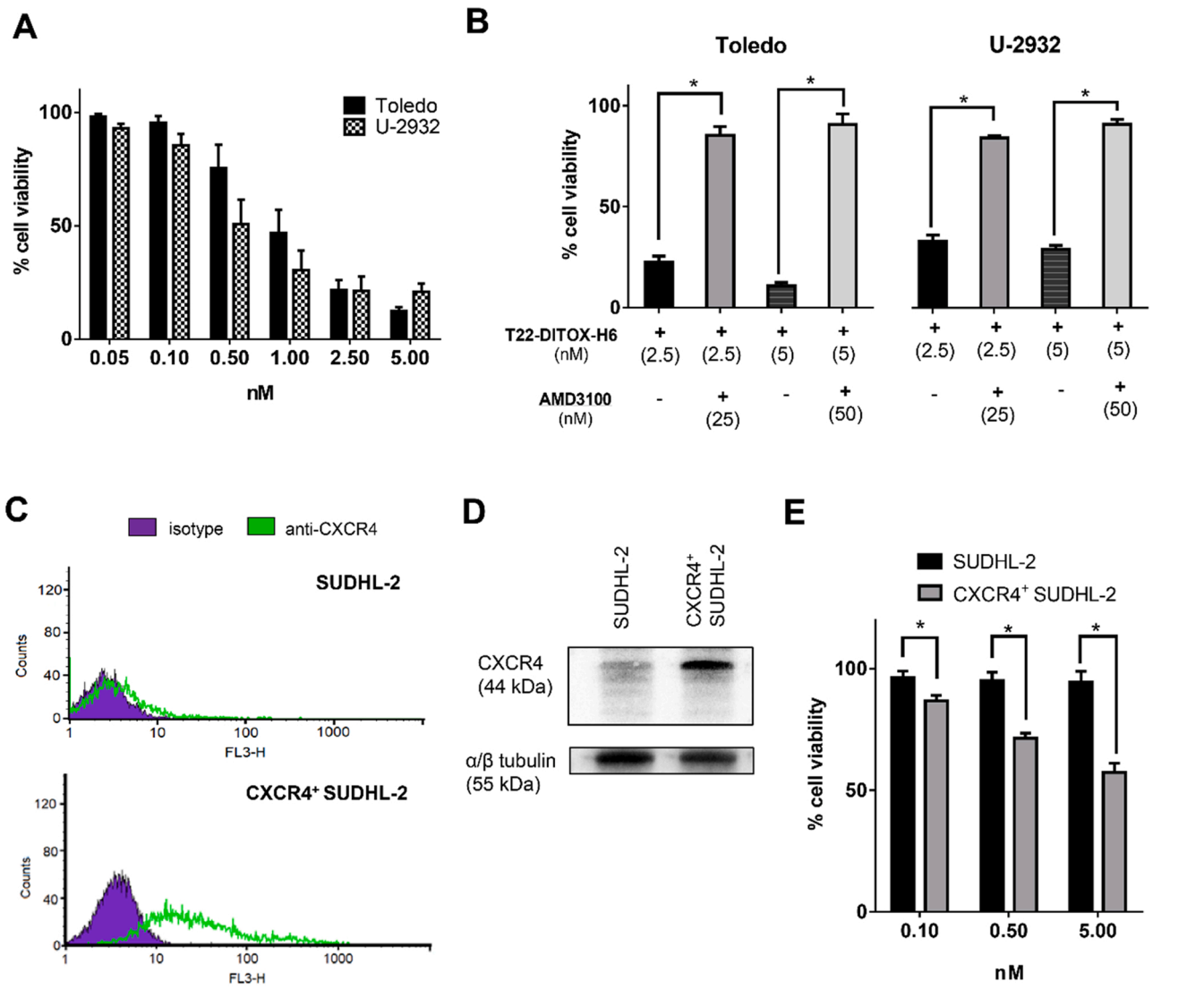

Fig. 1. T22-DITOX-H6 specific cytotoxicity in human CXCR4$^+$ DLBCL cell lines. (A) Cell viability assays performed after 48 h of T22-DITOX-H6 incubation at different concentrations (0.05–5.00 nM) in Toledo and U-2932 cells. (B) Competition assays in Toledo and U-2932 cells with or without pretreating with the antagonist of CXCR4 AMD3100 followed by the nanoparticle incubation for 48 h (ratio 10 AMD3100: 1 T22-DITOX-H6). (C-D) CXCR4 determination in SUDHL-2 and CXCR4$^+$ SUDHL-2 cells by flow cytometry and Western blot. In panel D, α/β tubulin antibody is used as endogen control. (E) Cell viability assays performed in SUDHL-2 and CXCR4$^+$ SUDHL-2 cells after 48 h of T22-DITOX-H6 incubation (0.10–5.00 nM). *p ≤ 0.05.

Link48 following the manufacturer's instructions. Representative pictures were taken using an Olympus DP73 digital camera and processed with the Olympus CellD Imaging 3.3 software at x400 or x1000 magnifications.

2.13. Hematological toxicity

Blood was obtained by intracardiac punction (25G) the day that immunocompetent mice were killed and blood samples were collected in EDTA-tubes for the hematological analysis using the BC-5000 Vet (Mindray, Madrid, Spain). This device allowed us to count the number of white blood cells (WBC), platelets (PLT) and red blood cells (RBC), but also the percentage and number of each type of WBC (neutrophils, lymphocytes, monocytes, eosinophils and basophils).

2.14. Hepatic and renal functionality

Blood collected in EDTA-tubes was centrifuged at 600*g* for 10 min at 4 ºC for obtaining plasma. Then, plasma samples were analyzed for determining the aspartate transaminase (AST), alanine transaminase (ALT) enzyme activities, as well as creatinine and uric acid levels, using commercial kits (ASTL ref. 20764949 322; ALTL ref. 20764957 322, CREJ2 ref. 04810716 190 and UA2 ref. 03183807 190, Roche Diagnostics) and adapted for a COBAS 6000 autoanalyzer (Roche Diagnostics).

2.15. Statistical analysis

All *in vitro* experiments were performed in triplicate and *in vivo* experiments at least in quadruplicates. Numerical data were expressed as mean ± standard error. Differences between groups were analyzed using the Mann-Whitney U test and were considered statistically significant at $p \leq 0.05$. Statistical calculations were performed using SPSS software v21.

3. Results

The first step was to assess the specific cytotoxic effect of the T22-DITOX-H6 therapeutic nanoparticle in human CXCR4$^+$ DLBCL cell lines. For that, we used two DLBCL cell lines (Toledo and U-2932) which

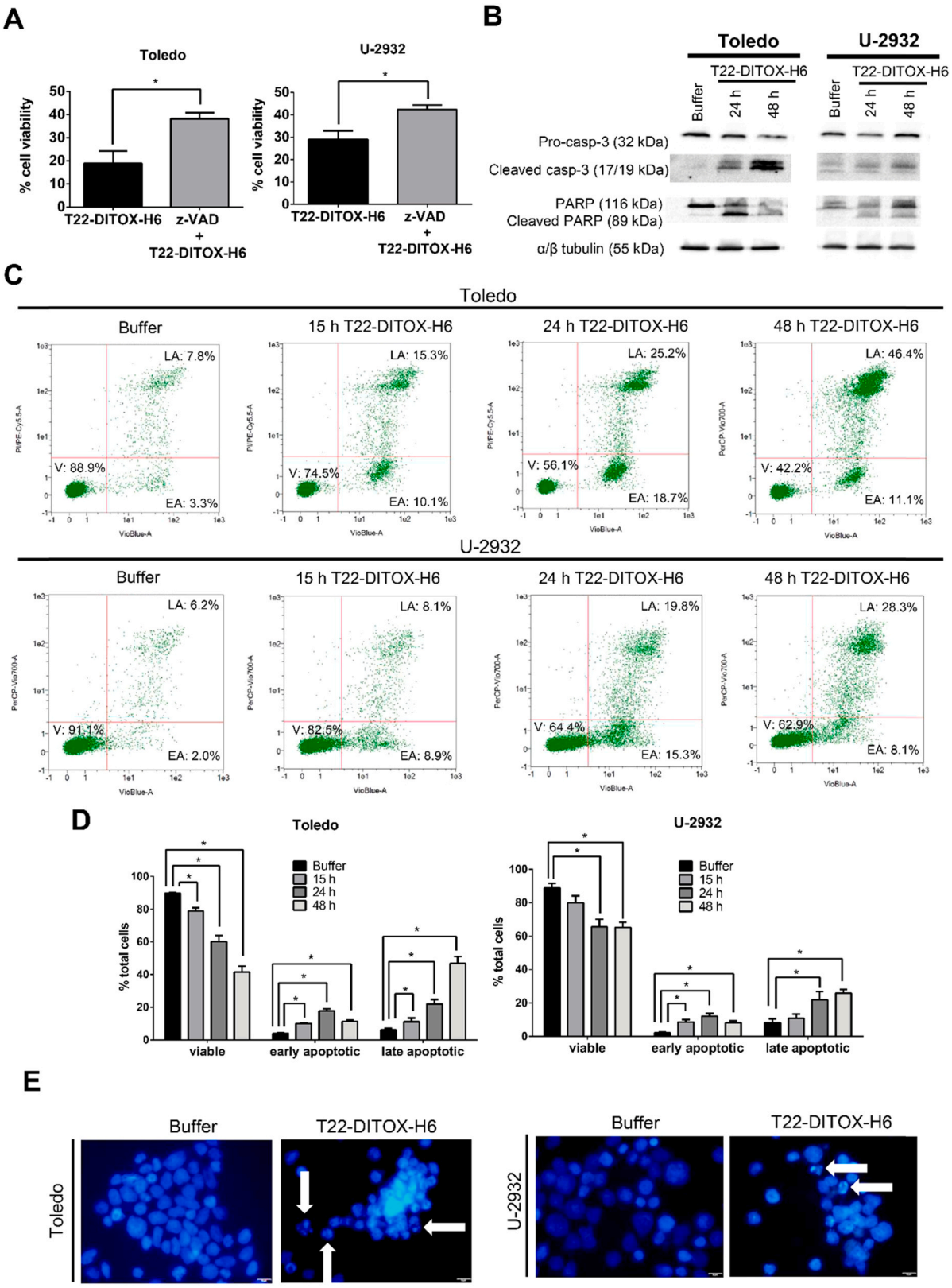

Fig. 2. Cell death mechanism induced by T22-DITOX-H6 in human CXCR4^{+} DLBCL cell lines. (A) Cell viability assays, pretreating Toledo and U-2932 cells with 100 μM of z-VAD-FMK pan caspase inhibitor, followed by the incubation of 5 nM of T22-DITOX-H6 for 48 h. (B) Western Blot analysis for the detection of pro-caspase-3, cleaved-caspase-3, full length Poly (ADP-ribose) polymerase (PARP) and cleaved PARP in Toledo and U-2932 cells, treated with buffer or 5 nM T22-DITOX-H6 for 24 h and 48 h. α/β tubulin antibody is used as endogen control. (C) Representative dot-plot from Annexin-PI assay showing the percent of viable cells (V), early apoptotic cells (EA) and late apoptotic cells (LA) in Toledo an U-2932 cells treated with buffer or 5 nM T22-DITOX-H6 at different time points (15 h, 24 h and 48 h) and (D) their respective quantification in triplicates. (E) DAPI staining images (1000X) of Toledo and U-2932 cells treated with buffer or 2.5 nM T22-DITOX-H6 for 48 h. White arrows point out apoptotic bodies. *$p \leq 0.05$.

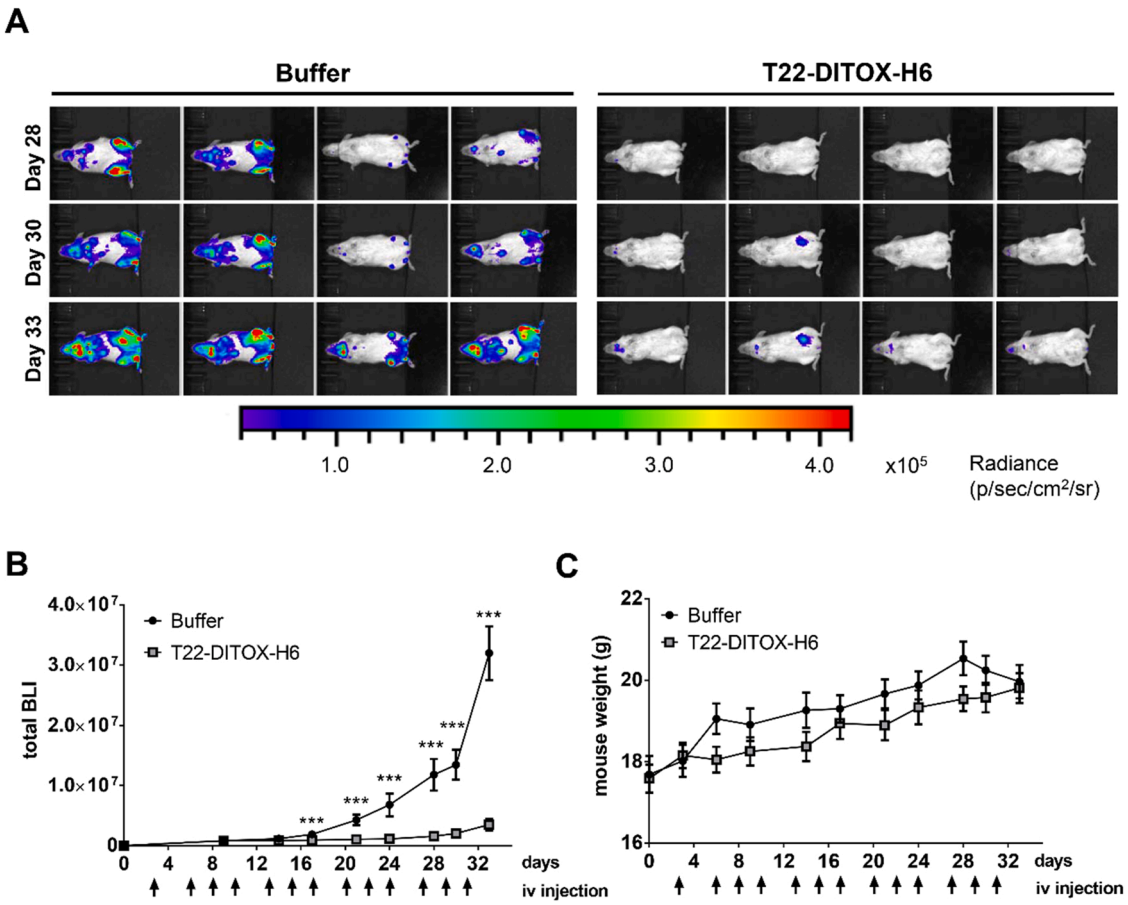

Fig. 3. *In vivo* antineoplastic effect of T22-DITOX-H6 in a disseminated CXCR4$^+$ DLBCL mouse model. (A) BLI emitted by Toledo-Luci cells from four representative mice of each group (buffer and T22-DITOX-H6) at days 28, 30 and 33. (B) BLI quantification of mice treated with buffer or T22-DITOX-H6 during the follow-up (n = 9/group). (C) Body weight of mice treated with buffer or T22-DITOX-H6 during the follow-up (n = 9/group). *** $p < 0.005$. BLI: bioluminescence imaging; iv: intravenous.

were previously reported to show high CXCR4 membrane expression [21,22]. After the exposure of these CXCR4$^+$ DLBCL cell lines to the nanoparticle for 48 h, cell viability was reduced in a concentration-dependent manner reaching 12.4 ± 1.6% and 20.8 ± 3.8% of cell viability in Toledo and U-2932 cells, respectively, at the maximum concentration of 5 nM (Fig. 1A).

As we wanted to determine whether the nanoparticle cytotoxic effect was due to its specific entrance through the CXCR4 receptor, Toledo and U-2932 cells were pretreated with the CXCR4 antagonist, AMD3100, following the nanoparticle addition. Cells treated with both AMD3100 and nanoparticle reversed significantly the cytotoxicity reaching up to 90.7% of cell viability compared to cells treated with the nanoparticle alone in both cell lines (Fig. 1B). Moreover, we used the parental SUDHL-2 cell line (CXCR4$^-$) and the CXCR4$^+$ SUDHL-2 cell line, previously transduced with the CXCR4 receptor, for testing the nanoparticle cytotoxic effect. After checking the absence of CXCR4 in SUDHL-2 cells and its presence in CXCR4$^+$ SUDHL-2 cells by flow cytometry and by Western Blot (Fig. 1C-D and Supplementary Figure 1), we demonstrated that T22-DITOX-H6 did not show cytotoxic effect in the negative-CXCR4 SUDHL-2 cell line (94.4 ± 4.4%) whereas it did in CXCR4$^+$ SUDHL-2 cells with 57.3 ± 3.8% of cell viability at 5 nM (Fig. 1E).

Furthermore, the cytotoxic effect of the nanoparticle in CXCR4$^+$ DLBCL cells was significantly reverted with the pretreatment of the caspase inhibitor z-VAD (2.0-fold in Toledo cells and 1.5-fold in U-2932 cells) (Fig. 2A). By Western blot, we observed the reduction of pro-caspase-3 together with the induction of cleaved caspase-3 as well as the presence of cleaved PARP in Toledo and U-2932 cells after 24 and 48 h incubation with 5 nM T22-DITOX-H6 (Fig. 2B and Supplementary Figure 1). Also, performing an Annexin/PI assay, we observed a significant increase of the percentage of cells in early and late apoptosis after 15, 24 and 48 h exposure with 5 nM of nanoparticle in CXCR4$^+$ DLBCL cells (Fig. 2C). Indeed, the peak of the percentage of early apoptotic cells was reached at 24 h (17.8 ± 1.2% of total cells in Toledo cells and 12.1 ± 1.6% of total cells in U-2932 cells) and subsequently the peak of late apoptosis was achieved after 48 h (46.7 ± 4.3% of total cells in Toledo cells and 25.8 ± 2.2% of total cells in U-2932 cells) (Fig. 2D). In addition, we observed, by DAPI staining, the formation of apoptotic bodies in the lymphoma cells treated with T22-DITOX-H6 for 48 h (Fig. 2E). These data suggest the induction of apoptosis by T22-DITOX-H6 in CXCR4$^+$ DLBCL cells.

At that point, we evaluated the nanoparticle cytotoxic effect in a CXCR4$^+$ DLBCL luminescent disseminated mouse model generated by intravenous injection of Toledo-Luci cells. Three days after cell injection, NODSCID mice were treated with buffer or 10 μg of T22-DITOX-H6, three days per week, in a total of thirteen doses. As observed by the bioluminescence (BLI) emitted by Toledo-Luci cells, the lymphoma was totally disseminated in buffer-treated mice at last days (days 30 and 33) compared to mice treated with T22-DITOX-H6 (Fig. 3A). The BLI quantification exhibited highly significant differences between mice treated with buffer and nanoparticle-treated mice, already at day 17 and until day 33, point at which the BLI signal was 9.1-fold times reduced in mice treated with T22-DITOX-H6 (Fig. 3B). Neither macroscopic alterations (not shown) nor loss of mouse weight was found in nanoparticle-treated mice (Fig. 3C). An *ex vivo* analysis of lymphoma-infiltrated organs at the end of treatment found that nanoparticle-treated animals showed a significant reduction of invading lymphoma cells, detected by

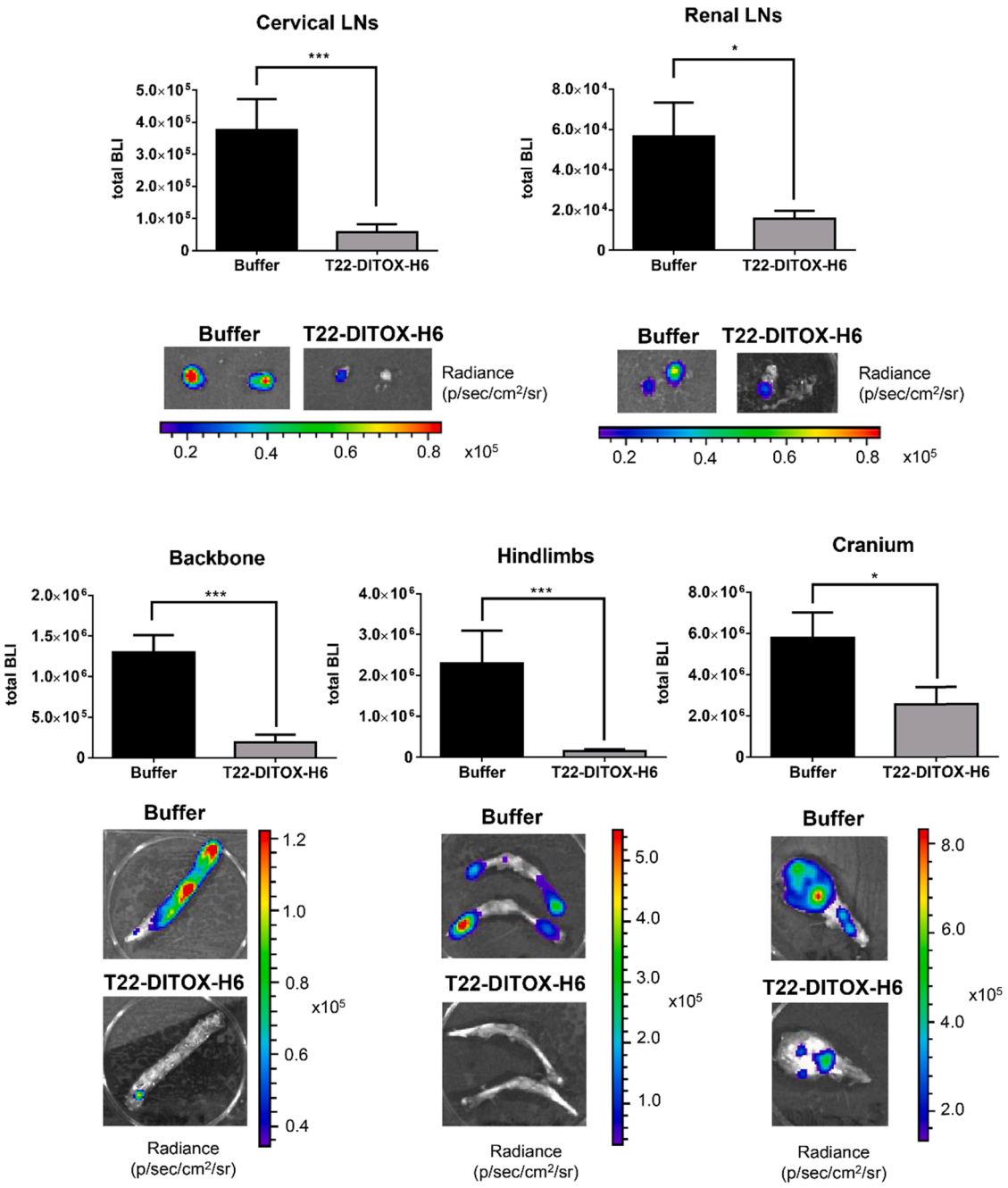

Fig. 4. *Ex vivo* antineoplastic effect of T22-DITOX-H6 in a disseminated CXCR4$^+$ DLBCL mouse model. BLI quantification and representative images of lymphoma-infiltrated organs (cervical LNs, renal LNs, backbone, hindlimbs and cranium) from Toledo-Luci mice treated either with buffer or T22-DITOX-H6 at the end of the experiment. *p ≤ 0.05, ***p ≤ 0.005. BLI: bioluminescence imaging; LNs: lymph nodes.

BLI, in cervical and renal LNs (6.6-fold and 3.6-fold, respectively) as well as in BM, including backbone, hind limbs and cranium (6.7-fold, 15.4-fold and 2.3-fold, respectively) (Fig. 4). Moreover, no histopathological alterations were found in hematoxylin and eosin (H&E) stained tissue sections of liver, spleen, kidneys, lungs and BM in nanoparticle-treated mice (Supplementary Figure 2).

Once we demonstrated the potent cytotoxic effect of the nanoparticle in human CXCR4$^+$ DLBCL cells *in vitro* and *in vivo* in immunocompromised mice, next step was to evaluate the effect of the nanoparticle in murine CXCR4$^+$ lymphoma cells and especially its toxicity (local, systemic and functional) in immunocompetent mice. First, we determined that murine A-20 cells expressed high levels of CXCR4 receptor in the cell membrane by IHC and flow cytometry (Fig. 5A-B). After exposure of these cells for 48 h to the nanoparticle, their viability was reduced up to 38.33 ± 16.4% at 5 nM (Fig. 5C). Moreover, the cytotoxic effect was significantly reverted (90.9 ± 15.9%) when cells were preincubated with AMD3100 followed by the nanoparticle addition, confirming that the T22-DITOX-H6 cytotoxic effect in murine A-20 cells was performed specifically through the CXCR4 receptor (Fig. 5D). As we reported with human Toledo and U-2932 cells, the incubation with T22-DITOX-H6 for 48 h produced the formation of apoptotic bodies in murine CXCR4$^+$ A-20 cells as well (Fig. 5E).

Then, we evaluated the *in vivo* antitumor effect of the nanoparticle in a SC A-20 mouse model generated in immunocompetent BALB/cByJ mice. When tumors were palpable (day 10), we started administering buffer or T22-DITOX-H6 three times per week until the first tumor of any

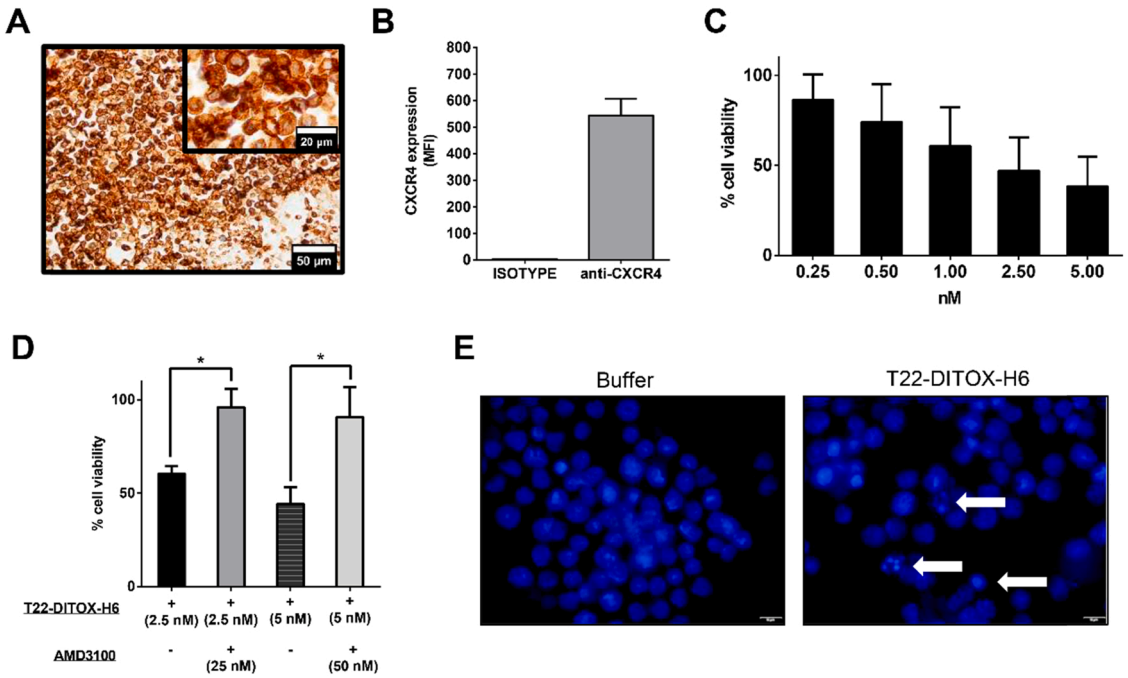

Fig. 5. T22-DITOX-H6 specific cytotoxicity in a murine CXCR4$^+$ lymphoma cell line. (A-B) CXCR4 determination by immunohistochemistry and flow cytometry in murine A-20 cells. Scale bars: main picture at 50 μm (400X) and the inset at 20 μm (1000X). (C) Cell viability assays measuring the T22-DITOX-H6 cytotoxicity in A-20 cells at different concentrations of the nanoparticle (0.25–5.00 nM) for 48 h. (D) Competition assays in A-20 cells with or without the pretreatment of the CXCR4 antagonist AMD3100 followed by the nanoparticle incubation for 48 h (ratio 10 AMD3100: 1 T22-DITOX-H6). MFI: mean fluorescence intensity. (E) DAPI staining pictures (1000X) of A-20 cells treated with buffer or 5 nM T22-DITOX-H6 for 48 h. White arrows point out apoptotic bodies. *p ≤ 0.05.

experimental animal reached 500 mm^3, point at which we stopped the administration (day 20). As a result, nanoparticle administration decreased tumor growth along time. At day 17, tumors reached a volume of 242.0 ± 25.9 mm^3 in buffer-treated mice, whereas tumor volume was significantly reduced in mice treated with the nanoparticle (121.4 ± 29.7 mm^3) (Fig. 6A). Analyzing the area under the curve (AUC) from day 14 to the end of the experiment, a significant 46.9% reduction of tumor size was observed in mice treated with T22-DITOX-H6 compared to control mice (Fig. 6B). In addition, mouse body weight was not altered by the nanoparticle administration (Fig. 6C) and no histopathological alterations were observed in spleen, liver, kidneys and BM from nanoparticle-treated mice (Fig. 6D).

Most importantly, we performed an exhaustive toxicity study to evaluate the potential clinical translation of the nanoparticle. This analysis showed a lack of significant differences between control and nanoparticle-treated mice regarding the number of WBC, PLT or RBC (Fig. 7A). Moreover, the percentage of cells in each WBC subtype (neutrophils, lymphocytes, monocytes, eosinophils and basophils) was not altered by nanoparticle treatment (Fig. 7B). We also checked the hepatic function by measuring the AST and ALT levels as well as the renal function determining creatinine and uric acid levels. These data showed the absence of hepatic and renal damage in mice treated with the nanoparticle since these parameters remained unaltered (Fig. 7C). Therefore, the T22-DITOX-H6 nanoparticle showed a selective cytotoxic effect in murine CXCR4$^+$ lymphoma cells without inducing on-target or off-target toxicity.

4. Discussion

Actively targeted nanoparticles are promising toxin-delivery systems. The T22-DITOX-H6 therapeutic nanoparticle has demonstrated not only a potent cytotoxic effect *in vitro* in CXCR4$^+$ DLBCL cells at the low nanomolar range, but also a high *in vivo* efficacy by blocking the lymphoma dissemination in the immunocompromised mice and reducing tumor growth in immunocompetent mice. This observation means that our nanoparticle targets and kills murine and human CXCR4$^+$ lymphoma cells independently of the presence of murine immune cells.

It has been reported that immunotoxins incorporating the diphtheria toxin can cause severe side effects. One example is the diphtheria toxin attached to interleukin-2 (denileukin diftitox), a drug approved by the FDA to treat cutaneous T-cell lymphoma; however, it was withdrawn from the market in 2014 because of severe side effects [23]. Afterwards, a novel immunotoxin containing diphtheria toxin was generated by replacing interleukin-2 by interleukin-3 so that they targeted leukemic stem cells. The combination of diphtheria toxin and interleukin-3 received the name of tagraxofusp-erzs, and it was approved by the FDA in 2018. Despite being in the market, several clinical trials using tagraxofusp-erzs reported serious adverse events in various hematologic neoplasms, including capillary leak syndrome (CLS) of grade ≤ 3 and three cases of fatal CLS especially in a trial for blastic plasmacytoid dendritic cell neoplasm (BPDCN). Moreover, across these trials, thrombocytopenia was also a significant side effect reaching grade ≤ 4 as well as transaminitis grade ≤ 3.[24]. Additionally, other immunotoxins containing diphtheria toxin domains that targeted CD3 or GM-CSFR in hematologic malignancies showed off-target toxicities in phase I/II clinical trials, including CLS, rare immunocompromised host infections or liver injury [25–27].

In contrast to immunotoxins, the selective diphtheria toxin delivery accomplished by our T22-DITOX-H6 nanoparticle offers a more effective selectivity to target cancer cells since the self-assembled T22-DITOX-H6 nanostructure incorporates multimeric T22 ligands for the CXCR4 receptor that enhance internalization in target cells compared to the only two ligands displayed by the immunotoxins [28,29]. Importantly, the multi-valency based on a large number of ligand moieties in the nanoparticle surface, confers super-selectivity to target cells, which means that T22-DITOX-H6 is able to interact with the CXCR4 receptor only when its density in the cell membrane is higher than a specific threshold [30,31]. As CXCR4$^+$ DLBCL cells usually show extremely higher levels of the receptor than normal hematopoietic cells (140-fold higher) [18], the

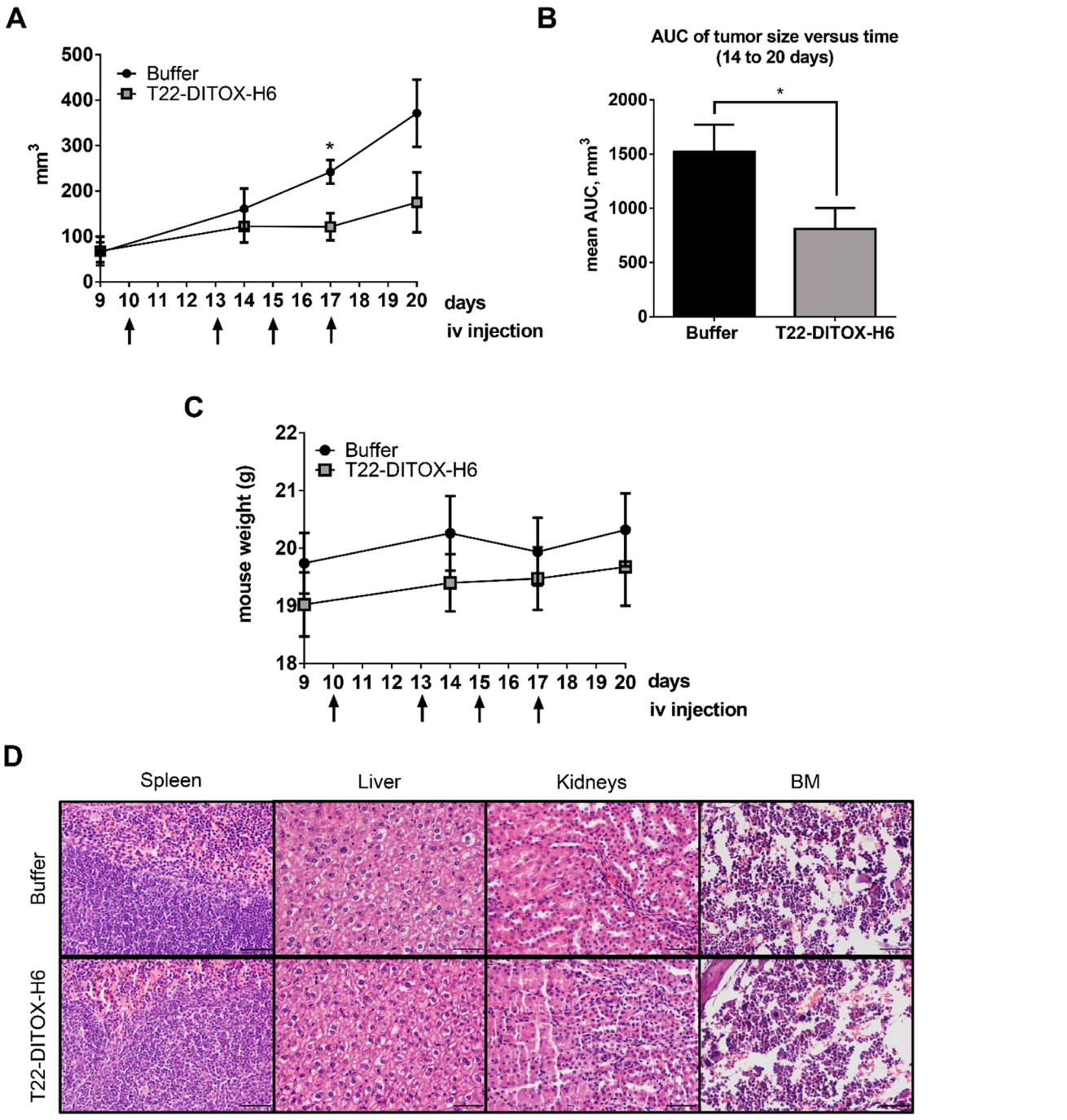

Fig. 6. T22-DITOX-H6 anti-tumor effect, and on-target and off-target toxicity in a SC mouse model bearing murine CXCR4$^+$ lymphoma cells. (A) A-20 SC tumor volume from mice treated with buffer (n = 5) or T22-DITOX-H6 (n = 4) during the whole experiment. (B) AUC quantification of tumor volume from 14 to 20 days in buffer and nanoparticle-treated mice. (C) Body weight follow-up of mice bearing A-20 SC tumors, treated with buffer and T22-DITOX-H6. (D) Hematoxylin and eosin staining from on target and off-target organs (spleen, liver, kidneys and BM). Scale bars: 50 μm. *p ≤ 0.05. AUC: area under the curve; BM: bone marrow; iv: intravenous.

super-selectivity property conferred by the T22-DITOX-H6 aims to avoid or dramatically minimize any possible toxicity in normal cells that express low or medium membrane CXCR4 levels.

Furthermore, the tight T22-DITOX-H6 construction in a single polypeptide chain, without any subsequent chemical conjugation, potentially avoids the premature release of the toxin in the mouse bloodstream [20]. Consequently, with this notion, we did not observe any histopathological alteration in non-lymphoma infiltrated organs in immunocompromised nor immunocompetent mice treated with the nanoparticle. Most importantly, the administration of T22-DITOX-H6 in immunocompetent mice did not show hepatic and renal functional alteration nor hematological on-target toxicity. Although murine and human white blood cells, especially monocytes and lymphocytes, express CXCR4 [32–34], the expression levels in those cells are much lower than those in human CXCR4$^+$ DLBCL cell lines, as we described in our previous works [21,22].

According to our strategy, other researchers also used nanoparticle drug delivery systems for targeted delivery of diphtheria toxin in breast cancer and melanoma, with high efficiency and precision *in vitro* and *in vivo* [35,36]. In addition, our group has previously demonstrated the

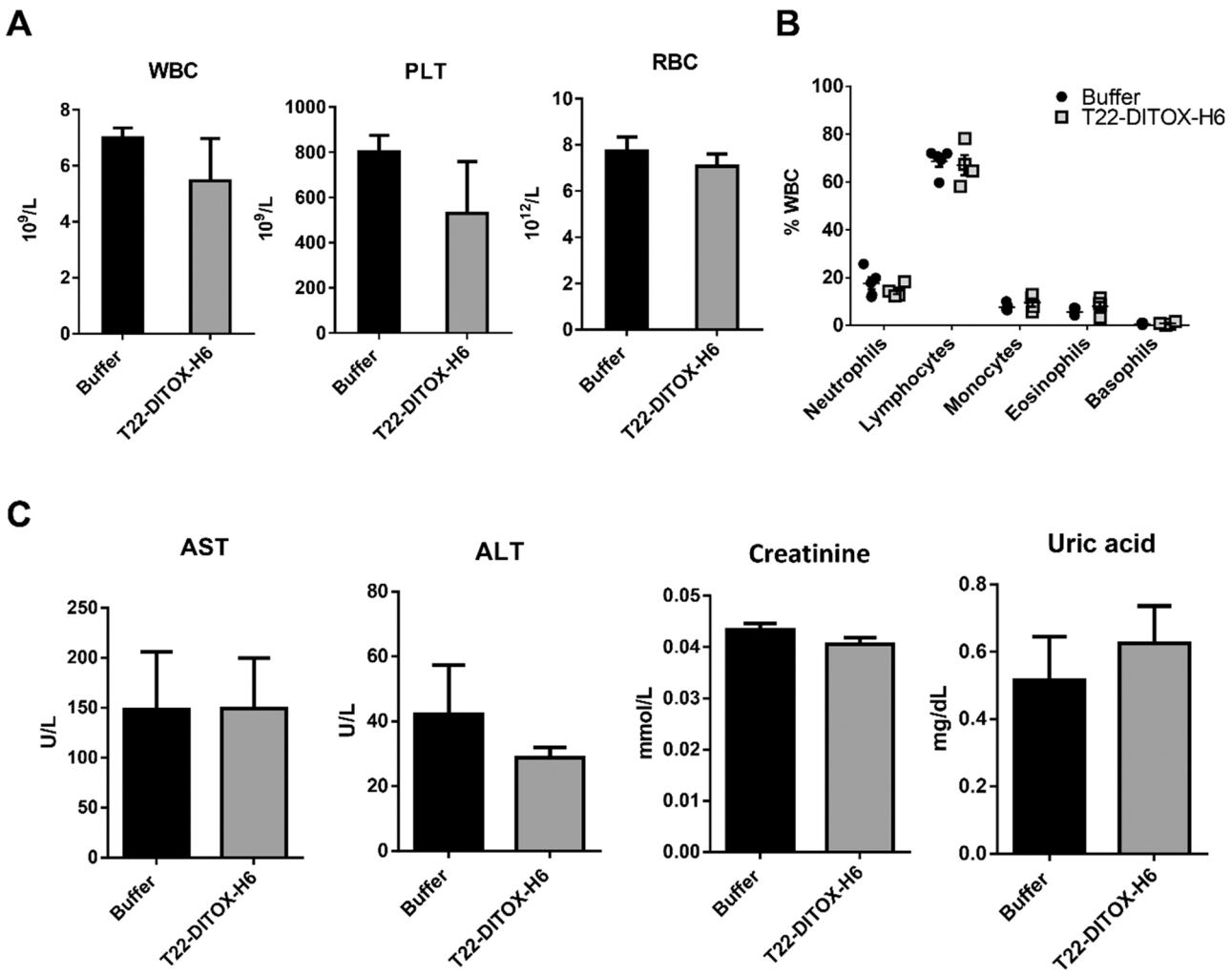

Fig. 7. Blood analysis and hepatic and renal functional evaluation from T22-DITOX-H6-treated mice bearing A-20 SC tumors. (A) Total number of WBC, PLT and RBC in mice treated with buffer or T22-DITOX-H6. (B) Percentage of the different types of WBC in buffer and nanoparticle-treated mice. (C) Measurement of the AST and ALT enzymes as well as creatinine and uric acid waste products for evaluation of hepatic and renal toxicity, respectively, in mice treated with buffer or T22-DITOX-H6. ALT: alanine aminotransferase; AST: aspartate aminotransferase; PLT: platelets; RBC: red blood cells WBC: white blood cells.

antitumor effect of T22-DITOX-H6 in CXCR4$^+$ colorectal and lymphoma SC mouse models as well as in a disseminated CXCR4$^+$ acute myeloid leukemia (AML) mouse model [20,21,37].

As a conclusion, we believe that the T22-DITOX-H6 diphtheria toxin delivery system that incorporates the natural toxin is capable of inducing cytotoxic killing of both dividing and non-dividing cells, as reported [38]. This effect shows specificity towards CXCR4$^+$ DLBCL cells, therefore, sparing the on-target and off-target toxicities showed by the immunotoxins. Thus, this toxin-based nanoparticle drug could be a good strategy to target and kill CXCR4$^+$ lymphoma cells from refractory or relapsed DLBCL patients.

CRediT authorship contribution statement

Conception and design: A.F., N.S., L.S.G., U.U., A.V., E.V., I.C. and R. M.; Development of methodology: A.F., A.G.L., Y.N., E.V.D., P.A. and L. A.C.; Acquisition of data: A.F., A.G.L., Y.N. and M.A.; Histopathological analysis: A.F. and A.G.; Analysis and interpretation of data: A.F., U.U., J. S., A.V., E.V., I.C. and R.M.; Drafted the manuscript: A.F.; Review and revision of manuscript: U.U., A.V., E.V., I.C. and R.M.; Study supervision: J.S., E.V., I.C. and R.M.

Declaration of conflicting interests

The authors declare the following financial interests/personal relationships which may be considered as potential competing interests: The authors declare the following financial interests/personal relationships which may be considered as potential competing interests: E.V., R. M. and A.V. are co-founders of Nanoligent, a company devoted to develop anticancer drugs based on proteins. U.U., E.V., A.V., R.M. and I. C. are cited as inventors in a patent application (EP11382005.4) covering the therapeutic use of T22. All other authors report no conflicts of interest in this work.

Acknowledgments

This work was supported by Instituto de Salud Carlos III (ISCIII, Co-funding from FEDER) [PI21/00150, PI18/00650, and EU COST Action CA 17 140 to R.M.; FIS PI20/01621, PI17/01246 and RD16/0011/0028 to J.S.; and PI20/00400 to U·U.]; Agencia Estatal de Investigación (AEI) and Fondo Europeo de Desarrollo Regional (FEDER) (grant BIO2016-76063-R, AEI/FEDER, UE) to A.V.; (grant PID2019-105416RB-I00/AEI/10.13039/501100011033) to E.V.; CIBER-BBN [CB06/01/1031 and 4NanoMets to R.M., VENOM4CANCER to A.V., NANOREMOTE to E.V. and NANOSCAPE to U·U.]; AGAUR [2017-SGR-865 to R.M., 2017-SGR-1395 to J.S. and 2017SGR-229 to A.V.]; Josep Carreras Leukemia

Research Institute [P/AG to R.M.]; La Marató TV3 [201 941-30-31-32 to J.S. and A.V.]; a grant from the Cellex Foundation, Barcelona [to J.S.]; a grant from the Generalitat de Catalunya CERCA Programme; U.U. is supported by Miguel Servet fellowship (CP19/00028) from Instituto de Salud Carlos III co-funded by Fondo Social Europeo (ESF investing in your future); L.A.C was supported by a postdoctoral fellowship from AECC (Spanish Association of Cancer Research, Spain); Y.N. was supported by a predoctoral fellowship (FI18/00268) from Instituto de Salud Carlos III. Finally, A.V. received an ICREA ACADEMIA Award supported by the Catalan Government.

We are also indebted to the ISCIII Networking Research Center on Bioengineering, Biomaterials and Nanomedicine (CIBER-BBN) and its ICTS Nanbiosis Platform for their funding. The bioluminescent follow-up of cancer cells and toxicity studies has been performed in the ICTS-141007 Nanbiosis Platform, using its CIBER-BBN Nanotoxicology Unit (http://www.nanbiosis.es/portfolio/u18-nanotoxicology-unit/). Protein production has been partially performed by the ICTS "NANBIOSIS", more specifically by the Protein Production Platform of CIBER-BBN/IBB (http://www.nanbiosis.es/unit/u1-protein-production-platform-ppp/).

Finally, we would like to acknowledge that the Graphical Abstract was created using biorender.com platform.

Appendix A. Supporting information

Supplementary data associated with this article can be found in the online version at doi:10.1016/j.biopha.2022.112940.

References

[1] J. Crombie, Classifying DLBCL subtypes for optimal treatment, Oncology 33 (2019), 686504.
[2] M. Crump, S.S. Neelapu, U. Farooq, E. Van Den Neste, J. Kuruvilla, J. Westin, B. K. Link, A. Hay, J.R. Cerhan, L. Zhu, S. Boussetta, L. Feng, M.J. Maurer, L. Navale, J. Wiezorek, W.Y. Go, C. Gisselbrecht, Outcomes in refractory diffuse large B-cell lymphoma: results from the international SCHOLAR-1 study, Blood 130 (2017) 1800–1808, https://doi.org/10.1182/blood-2017-03-769620.
[3] C. Sarkozy, L.H. Sehn, Management of relapsed/refractory DLBCL, Best Pract Res Clin. Haematol. 31 (2018) 209–216, https://doi.org/10.1016/j.beha.2018.07.014.
[4] V. MacDonald, Chemotherapy: managing side effects and safe handling, Can. Vet. J. 50 (2009) 665–668.
[5] F. Foroughinia, S. Baniasadi, S. Seifi, F. Fahimi, Vincristine-induced seizure potentiated by itraconazole following RCHOP chemotherapy for diffuse large B-cell lymphoma, Curr. Drug Saf. 7 (2012) 372–374, https://doi.org/10.2174/157488612805076633.
[6] M.A. Fridrik, U. Jaeger, A. Petzer, W. Willenbacher, F. Keil, A. Lang, J. Andel, S. Burgstaller, O. Krieger, W. Oberaigner, K. Sihorsch, R. Greil, Cardiotoxicity with rituximab, cyclophosphamide, non-pegylated liposomal doxorubicin, vincristine and prednisolone compared to rituximab, cyclophosphamide, doxorubicin, vincristine, and prednisolone in frontline treatment of patients with diffuse large B-cell lymphoma: a randomised phase-III study from the Austrian Cancer Drug Therapy Working Group [Arbeitsgemeinschaft Medikamentöse Tumortherapie AGMT](NHL-14), Eur. J. Cancer 58 (2016) 112–121, https://doi.org/10.1016/j.ejca.2016.02.004.
[7] S. Limat, K. Demesmay, L. Voillat, Y. Bernard, E. Deconinck, A. Brion, A. Sabbah, M.C. Woronoff-Lemsi, J.Y. Cahn, Early cardiotoxicity of the CHOP regimen in aggressive non-Hodgkin's lymphoma, Ann. Oncol. 14 (2003) 277–281, https://doi.org/10.1093/annonc/mdg070.
[8] C. Mörth, A. Valachis, A.A. Sabaa, D. Molin, M. Flogegård, G. Enblad, Does the omission of vincristine in patients with diffuse large B cell lymphoma affect treatment outcome? Ann. Hematol. 97 (2018) 2129–2135, https://doi.org/10.1007/s00277-018-3437-z.
[9] S. Hamamichi, T. Fukuhara, N. Hattori, Immunotoxin screening system: a rapid and direct approach to obtain functional antibodies with internalization capacities, Toxins 12 (2020), E658, https://doi.org/10.3390/toxins12100658.
[10] E.Y. Jen, X. Gao, L. Li, L. Zhuang, N.E. Simpson, B. Aryal, R. Wang, D. Przepiorka, Y.L. Shen, R. Leong, C. Liu, C.M. Sheth, S. Bowen, K.B. Goldberg, A.T. Farrell, G. M. Blumenthal, R. Pazdur, FDA approval summary: tagraxofusp-erzs for treatment of blastic plasmacytoid dendritic cell neoplasm, Clin. Cancer Res. 26 (2020) 532–536, https://doi.org/10.1158/1078-0432.CCR-19-2329.
[11] R.J. Kreitman, C. Dearden, P.L. Zinzani, J. Delgado, L. Karlin, T. Robak, D. E. Gladstone, P. le Coutre, S. Dietrich, M. Gotic, L. Larratt, F. Offner, G. Schiller, R. Swords, L. Bacon, M. Bocchia, K. Bouabdallah, D.A. Breems, A. Cortelezzi, S. Dinner, M. Doubek, B.T. Gjertsen, M. Gobbi, A. Hellmann, S. Lepretre, F. Maloisel, F. Ravandi, P. Rousselot, M. Rummel, T. Siddiqi, T. Tadmor, X. Troussard, C.A. Yi, G. Saglio, G.J. Roboz, K. Balic, N. Standifer, P. He, S. Marshall, W. Wilson, I. Pastan, N.-S. Yao, F. Giles, Moxetumomab pasudotox in relapsed/refractory hairy cell leukemia, Leukemia 32 (2018) 1768–1777, https://doi.org/10.1038/s41375-018-0210-1.
[12] C.F. Nobre, M.J. Newman, A. DeLisa, P. Newman, Moxetumomab pasudotox-tdfk for relapsed/refractory hairy cell leukemia: a review of clinical considerations, Cancer Chemother. Pharmacol. 84 (2019) 255–263, https://doi.org/10.1007/s00280-019-03875-6.
[13] G. Aruna, Immunotoxins: a review of their use in cancer treatment, J. Stem Cells Regen. Med. 1 (2006) 31–36, https://doi.org/10.46582/jsrm.0101005.
[14] H. Donaghy, Effects of antibody, drug and linker on the preclinical and clinical toxicities of antibody-drug conjugates, MAbs 8 (2016) 659–671, https://doi.org/10.1080/19420862.2016.1156829.
[15] J. Chen, Z.Y. Xu-Monette, L. Deng, Q. Shen, G.C. Manyam, A. Martinez-Lopez, L. Zhang, S. Montes-Moreno, C. Visco, A. Tzankov, L. Yin, K. Dybkaer, A. Chiu, A. Orazi, Y. Zu, G. Bhagat, K.L. Richards, E.D. Hsi, W.W.L. Choi, J.H. van Krieken, J. Huh, M. Ponzoni, A.J.M. Ferreri, X. Zhao, M.B. Møller, J.P. Farnen, J.N. Winter, M.A. Piris, L. Pham, K.H. Young, Dysregulated CXCR4 expression promotes lymphoma cell survival and independently predicts disease progression in germinal center B-cell-like diffuse large B-cell lymphoma, Oncotarget 6 (2015) 5597–5614, https://doi.org/10.18632/oncotarget.3343.
[16] M.J. Moreno, R. Bosch, R. Dieguez-Gonzalez, S. Novelli, A. Mozos, A. Gallardo, M.Á. Pavón, M.V. Céspedes, A. Grañena, M. Alcoceba, O. Blanco, M. Gonzalez-Díaz, J. Sierra, R. Mangues, I. Casanova, CXCR4 expression enhances diffuse large B cell lymphoma dissemination and decreases patient survival, J. Pathol. 235 (2015) 445–455, https://doi.org/10.1002/path.4446.
[17] H. Du, L. Zhang, G. Li, W. Liu, W. Tang, H. Zhang, J. Luan, L. Gao, X. Wang, CXCR4 and CCR7 expression in primary nodal diffuse large B-cell lymphoma-A clinical and immunohistochemical study, Am. J. Med. Sci. 357 (2019) 302–310, https://doi.org/10.1016/j.amjms.2019.01.008.
[18] K. Pansy, J. Feichtinger, B. Ehall, B. Uhl, M. Sedej, D. Roula, B. Pursche, A. Wolf, M. Zoidl, E. Steinbauer, V. Gruber, H.T. Greinix, K.T. Prochazka, G.G. Thallinger, A. Heinemann, C. Beham-Schmid, P. Neumeister, T.M. Wrodnigg, K. Fechter, A. J. Deutsch, The CXCR4-CXCL12-axis is of prognostic relevance in DLBCL and its antagonists exert pro-apoptotic effects in vitro, Int. J. Mol. Sci. 20 (2019), E4740, https://doi.org/10.3390/ijms20194740.
[19] R.J. Collier, Understanding the mode of action of diphtheria toxin: a perspective on progress during the 20th century, Toxicon 39 (2001) 1793–1803, https://doi.org/10.1016/s0041-0101(01)00165-9.
[20] L. Sánchez-García, N. Serna, P. Álamo, R. Sala, M.V. Céspedes, M. Roldan, A. Sánchez-Chardi, U. Unzueta, I. Casanova, R. Mangues, E. Vázquez, A. Villaverde, Self-assembling toxin-based nanoparticles as self-delivered antitumoral drugs, J. Control Release 274 (2018) 81–92, https://doi.org/10.1016/j.jconrel.2018.01.031.
[21] A. Falgàs, V. Pallarès, U. Unzueta, M.V. Céspedes, I. Arroyo-Solera, M.J. Moreno, J. Sierra, A. Gallardo, M.A. Mangues, E. Vázquez, A. Villaverde, R. Mangues, I. Casanova, A CXCR4-targeted nanocarrier achieves highly selective tumor uptake in diffuse large B-cell lymphoma mouse models, Haematologica 105 (2020) 741–753, https://doi.org/10.3324/haematol.2018.211490.
[22] A. Falgàs, V. Pallarès, U. Unzueta, Y. Núñez, J. Sierra, A. Gallardo, L. Alba-Castellón, M.A. Mangues, P. Álamo, A. Villaverde, E. Vázquez, R. Mangues, I. Casanova, Specific cytotoxic effect of an auristatin nanoconjugate towards CXCR4+ diffuse large B-cell lymphoma cells, Int. J. Nanomed. 16 (2021) 1869–1888, https://doi.org/10.2147/IJN.S289733.
[23] J.-S. Kim, S.-Y. Jun, Y.-S. Kim, Critical issues in the development of immunotoxins for anticancer therapy, J. Pharm. Sci. 109 (2020) 104–115, https://doi.org/10.1016/j.xphs.2019.10.037.
[24] O. Alkharabsheh, A.E. Frankel, Clinical activity and tolerability of SL-401 (Tagraxofusp): recombinant diphtheria toxin and interleukin-3 in hematologic malignancies, Biomedicines 7 (2019), E6, https://doi.org/10.3390/biomedicines7010006.
[25] A.E. Frankel, B.L. Powell, P.D. Hall, L.D. Case, R.J. Kreitman, Phase I trial of a novel diphtheria toxin/granulocyte macrophage colony-stimulating factor fusion protein (DT388GMCSF) for refractory or relapsed acute myeloid leukemia, Clin. Cancer Res. 8 (2002) 1004–1013.
[26] A.E. Frankel, J.H. Woo, C. Ahn, F.M. Foss, M. Duvic, P.H. Neville, D.M. Neville, Resimmune, an anti-CD3ε recombinant immunotoxin, induces durable remissions in patients with cutaneous T-cell lymphoma, Haematologica 100 (2015) 794–800, https://doi.org/10.3324/haematol.2015.123711.
[27] X. Mei, J. Chen, J. Wang, J. Zhu, Immunotoxins: targeted toxin delivery for cancer therapy, Pharm. Fronts 01 (2019) e33–e45, https://doi.org/10.1055/s-0039-1700507.
[28] V. Pallarès, U. Unzueta, A. Falgàs, L. Sánchez-García, N. Serna, A. Gallardo, G. A. Morris, L. Alba-Castellón, P. Álamo, J. Sierra, A. Villaverde, E. Vázquez, I. Casanova, R. Mangues, An Auristatin nanoconjugate targeting CXCR4+ leukemic cells blocks acute myeloid leukemia dissemination, J. Hematol. Oncol. 13 (2020) 36, https://doi.org/10.1186/s13045-020-00863-9.
[29] J.L. Sanchez-Trincado, M. Gomez-Perosanz, P.A. Reche, Fundamentals and methods for T- and B-cell epitope prediction, J. Immunol. Res. 2017 (2017), 2680160, https://doi.org/10.1155/2017/2680160.
[30] M. Liu, A. Apriceno, M. Sipin, E. Scarpa, L. Rodriguez-Arco, A. Poma, G. Marchello, G. Battaglia, S. Angioletti-Uberti, Combinatorial entropy behaviour leads to range selective binding in ligand-receptor interactions, Nat. Commun. 11 (2020) 4836, https://doi.org/10.1038/s41467-020-18603-5.
[31] F.J. Martinez-Veracoechea, D. Frenkel, Designing super selectivity in multivalent nano-particle binding, Proc. Natl. Acad. Sci. USA 108 (2011) 10963–10968, https://doi.org/10.1073/pnas.1105351108.

[32] R. Förster, E. Kremmer, A. Schubel, D. Breitfeld, A. Kleinschmidt, C. Nerl, G. Bernhardt, M. Lipp, Intracellular and surface expression of the HIV-1 coreceptor CXCR4/fusin on various leukocyte subsets: rapid internalization and recycling upon activation, J. Immunol. 160 (1998) 1522–1531.
[33] C. Martin, P.C.E. Burdon, G. Bridger, J.-C. Gutierrez-Ramos, T.J. Williams, S. M. Rankin, Chemokines acting via CXCR2 and CXCR4 control the release of neutrophils from the bone marrow and their return following senescence, Immunity 19 (2003) 583–593, https://doi.org/10.1016/S1074-7613(03)00263-2.
[34] R. Schabath, G. Müller, A. Schubel, E. Kremmer, M. Lipp, R. Förster, The murine chemokine receptor CXCR4 is tightly regulated during T cell development and activation, J. Leukoc. Biol. 66 (1999) 996–1004, https://doi.org/10.1002/jlb.66.6.996.
[35] M. He, Y. Wang, X. Chen, Y. Zhao, K. Lou, Y. Wang, L. Huang, X. Hou, J. Xu, X. Cai, Y. Cheng, M. Lan, Y. Yang, F. Gao, Spatiotemporally controllable diphtheria toxin expression using a light-switchable transgene system combining multifunctional nanoparticle delivery system for targeted melanoma therapy, J. Control Release 319 (2020) 1–14, https://doi.org/10.1016/j.jconrel.2019.12.015.
[36] X. Hou, C. Shou, M. He, J. Xu, Y. Cheng, Z. Yuan, M. Lan, Y. Zhao, Y. Yang, X. Chen, F. Gao, A combination of LightOn gene expression system and tumor microenvironment-responsive nanoparticle delivery system for targeted breast cancer therapy, Acta Pharm. Sin. B 10 (2020) 1741–1753, https://doi.org/10.1016/j.apsb.2020.04.010.
[37] V. Pallarès, Y. Núñez, L. Sánchez-García, A. Falgàs, N. Serna, U. Unzueta, A. Gallardo, L. Alba-Castellón, P. Álamo, J. Sierra, A. Villaverde, E. Vázquez, I. Casanova, R. Mangues, Antineoplastic effect of a diphtheria toxin-based nanoparticle targeting acute myeloid leukemia cells overexpressing CXCR4, J. Control Release 335 (2021) 117–129, https://doi.org/10.1016/j.jconrel.2021.05.014.
[38] C. Alewine, R. Hassan, I. Pastan, Advances in anticancer immunotoxin therapy, Oncologist 20 (2015) 176–185, https://doi.org/10.1634/theoncologist.2014-0358.